Numerical Evaluation of Solar Irradiance Attenuation for Concentrating Solar Power Systems: Case of Morocco

Abdelkader Beyoud*‡, Najem Hassanain**, Ahmed Bouhaouss*

*Laboratory of Nano Structures, Process Engineering and Environment, Faculty of Sciences, Mohammed V University - Rabat, Morocco

**Physics of Material Laboratory (LPM), Faculty of Sciences, Mohammed V University - Rabat, Morocco

(ay.beyoud@gmail.com)

‡ Corresponding Author; Abdelkader Beyoud, Laboratory of Nano Structures, Process Engineering and Environment, Faculty of Sciences, Mohammed V University - Rabat, Morocco, Tel: +212 661 36 55 66

Abstract- Aerosol Optical Depth (AOD) data analysis in relation with turbidity Linke factor and heliostat atmospheric attenuation of solar beam irradiation assessment are critical elements for suitable optimal management and sizing of energy systems installation using solar tower technology. This paper demonstrates that AOD Weibull distribution along with the Kolmogorov-Smirnov test and the coefficient of variation index is capable of describing accurately the attenuation beam solar irradiation in two timescales conditions; the regular rainfall period and the irregular one. The Weibull distribution parameters are determined based on measured tri-hourly mean aerosols optical depth data in times-series for a decade and a year. The data were collected from MACC reanalysis aerosol, at the climates under effect of Mediterranean, oceanic, continental, desert, Sahara and mountain influence of represented by Rabat, Oujda, Ouarzazate, Er-Rachidia and S'mara (Morocco). For each site, a sample of 31936 tri-hourly time series from AOD data for over 10 years was analyzed. Two climate zones have been defined; the northern zone with a fluctuating Linke turbidity factor around 3.5 (highest 5.5 in august in Oujda and lowest 3.13 in January in Ouarzazate), and the southern zone 'S'mara' where it fluctuates around 4.5 (highest 6 in July and lowest 3.6 in January). The obtained results are interpreted and an account of the major findings including prospective applications of the present study is given and discussed. It is also pointed out that this study might be generalized to the locations with similar environmental conditions.

Keywords Attenuation solar assessment, Turbidity Linke factor, Aerosol Optical Depth, Weibull Distribution, Solar Tower Power

1. Introduction

Recently, there has been a growing interest in thermodynamic solar energy conversion in the world. Among solar energy conversion systems, concentrating solar energy is a very promising technology, including the solar Tower Power mainly, because it provides high temperature, for generating electrical high voltage and/or producing hydrogen. Nevertheless, this technology is confronted by high atmospheric aerosol content, in two ways. The first one, from the top atmosphere to heliostat in the ground due to scattering and absorption aerosols and water vapor atmospheric contents [1]; Secondly, it is constrained by those particles in the extra path travelling where the irradiation is reflected from the heliostat to the receiver tower.

The attenuation of solar radiation is an important key in the assessment of the solar energy resources studies at considered site. It is valued by several coefficient and factors such as the angstroms exponent, or the Linke turbidity coefficient. An important review in this case is presented by Eltbaakh et al. [2]. It takes into account both the atmospheric aerosol and water vapor content in the new formulation of Ineichen [3]. The turbidity Linke coefficient was introduced by Linke in 1922; it is related to the number of ideal superimposed atmospheres leading to the same attenuation than real atmosphere [4]. Even if it is easy to retrieve the water vapor measurement data from climatological

laboratory, or specialized satellites [5], it is not the same accessibilities for the AOD measurement. In 2008, with an aim to circumvent this difficulty, an approach was proposed based on two different models; the radiative transfer model and clear sky model. They describe a conversion function associated with the aerosol optical depth, the water vapor column and the Linke atmospheric turbidity factor.

Currently, widespread studies are being conducted in many parts of the world to evaluate and model solar potential. Markovian approaches that contributed to the random fluctuations model in solar radiation are worth considering. More topical studies have focused on the randomness model of solar radiation using neural networks and fractal analysis. Some works have used insolation [6-10] and others have used climatological data [11-15]. Furthermore to model the main components solar irradiance on clear and dry sky, researchers have also employed radiative transfer models (RTM).

In order to contribute to the realization of an aerosol atlas of Morocco similar to the studies carried out on Finnish wind atlas [16] and Saudi Arabia solar radiation atlas [17], in this work we demonstrate that the Aerosol Optical Depth (AOD) can be achieved by the Weibull distribution model which is a special case denoted by Generalized Extreme Value type III. The second exam of Kolmogorov Simonov critical value is related to the maximum likelihood estimation method which is a mathematically validated. The Weibull probability distribution function (PDF) can be used effectively to analyze skewness data sets and can provide comparable results, monthly averaged as small and moderate sized samples [18]. In general, this study aims firstly at evaluating the aerosols optical depth, and the attenuation the solar radiation with the help of statistical modelling. In the second phase, a comparative study of the solar attenuations evolutions of the five Moroccan sites representing particular climates in accordance with their rainfall periods will be carried out and discussed.

2. Materials and Methods

Atmospheric gases, clouds and aerosols absorb and diffuse solar radiation in all directions. A part of radiation is reflected towards the cosmic space. Another part passes through the atmosphere and reaches the surface of the earth. As shown in figure 1, The solar radiation reaching the surface will then be partially absorbed and reflected by various materials, such as dust, snow, sand and sea salt. The radiation reflected by the surface will then be scattered by the atmosphere and a part will be returned to the surface of the earth. This process of interaction with particles which exist between the surface and the atmosphere is continuous. This leads to an increase in diffused radiation at the surface relative to an ideal surface absorbing any incident solar radiation.

The Solar power plant performance is influenced by atmospheric attenuation at different temporal resolutions related to aerosol present in the atmosphere environments of the plant. The first one between the top of atmosphere (TOA) and the ground, where space was assessed by the Linke

Trouble factor (T_L), and the second attenuation between the heliostat (hi) and the receiver tower, exactly on the slant range A(%).
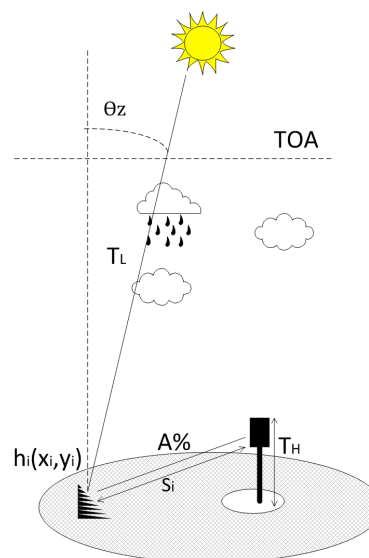

Fig. 1. Schematic diagram of the path traveling the beam solar irradiation from TOA to receiver Tower.

The two parameters evaluated intermediately the AOD, thus, the most accurate two-parameter Weibull PDF (next section) method to represent the AOD data collected in each of selected locality.

In addition this assessment was accomplished during two different timescales, the first concerned a period when the rainfall is regular, the second timescales concerned the irregular rainfall period described by the fine mode fraction (FMF) coefficient, explaining that the atmosphere contains coarse particles if it is low and vice versa [19], to report that the FMF with in correlation relationship to rainfall.

2.1. Atmospheric Solar Attenuation Related to the Solar Tower

As mentioned previously, the AOD is an important key on the solar attenuation from ground until the top of atmosphere and is useful in the studies such as radiative forcing, aerosol dispersion, and remote sensing correction. Generally the AOD measurement is usually unavailable for the direct determination of Linke turbidity factor and the average attenuation loss in the lower atmospheric boundary layer is used for the designed solar heliostat field layout. The Linke turbidity values T_L are then calculated from the beam irradiance on the basis of the best multivariable fit correlation in regard to the radiative transfer calculation. T_L is measured from the conversion function versus the atmospheric water vapor content (Wp) and aerosol optical depth at 550 nm (δ_{550}), at sea level and for an air mass AM=2 [20]. Ineichen [21] pointed out that the inverse function can be used to convert the Linke turbidity T_L to the aerosol optical depth.

On the other hand, the heliostat field concentrates the beam normal irradiance on the top of a central tower; in

accordance with the power of the plant, the solar field achieved a reflective surface up to several million of meter square. The solar radiation reflected by the distant heliostats to the receiver, undergoes a more or less intense weakening giving from the density of the aerosols present along their optical path. This extinction is added to the different optical losses of the solar field [22]. In the expected sites for CSP projects, the aerosol represents a particular variability range. Thus, it is a sensitivity parameter effect to the CSP plant production, which should have study interest and analysis sensitivity.

The canonical correlation analysis suggests that the air mass doesn't have a strong impact on solar attenuation from heliostat to receiver; though, it is obviously worth considering in the slant range and the aerosol optical depth AOD [23].

The analysis of atmospheric aerosol radiative parameters at the local level of two solar photometric stations, Oujda and Ouarzazate, of the AERONET were studied [24]. By employing the apparatus for measuring the extinction coefficient of the atmosphere in grouping to sun photometer the atmospheric attenuation have been described for southeast Spain [25]. It may provide a motive for the researchers of the related countries to conducting an atlas of AOD attenuation.

In addition to the attenuation analysis, the Ångström exponent parameter might also be evaluated [26]. This key parameter can give knowledge about the characterization of particles regarding to AOD contents. A high average value means existence of fine particles in the atmosphere and vice versa [27]. In the statistical point of view, likewise the measurements of all the random variables in various fields, the AOD measurements are expected to be described by the probability distribution function (PDF) [28, 29].

2.2. Probability Distribution Function (PDF) Analysis

The usually distributions used to describe atmospheric variables are normal and lognormal functions [30, 31], and [32]. Widely the lognormal distribution was applied, to characterize the statistical behaviors of measured AOD [33], [34]. A more difficult parameterization reaches more accurate distribution characteristics; however, it increases the application difficulty [35].

AERONET data based, O'Neill et al. has confirmed that the lognormal distribution is most representative than the normal distribution, so the geometric mean is more significant to describe the distribution average. Liu validate the recovered satellite AOD data measurements through lognormal distribution. However, he introduced the effect of different time scales on the PDF lognormal distribution and he demonstrates that the histogram of the AOD measurement data show a positive skewness [36]. Stability analysis was achieved for multi-timescale AOD using Aeronet data [37]. The Weibull PDF can be considered an appropriate distribution function for modeling statistically the aerosol optical depth data because it gives a good fitness to the measurements data at the ground surface up to the top atmosphere. The Weibull distribution can be characterized by

its probability density function f (δ_{550}) and its cumulative distribution function F (δ_{550}) is given as:

$$F\left(\delta_{550} \mid \alpha, \beta\right) = 1 - \exp\left(-\left(\frac{\delta_{550}}{\alpha}\right)^{\beta}\right) \qquad (1)$$

Where, (α, β) are respectively the scale parameter; and the shape parameter. The mathematical expression Maximum Likelihood Estimation method (MLM) is a function of the variable δ_{550}; the AOD data measured at wavelength 550 nm in time series format. The MLM approach is resolved through numerical iterations.

In order to validate for PDF proposal adequation for the available AOD data, Kolmogorov-Smirnov exam for fitting goodness hypothesis is considered, (usually used for wind speed studies) [38]. The test method applied to "n" bins of AOD data histogram, verifies the hypothesis that a data set is really represented by a Weibull distribution with known shape and scale parameters. Then, it calculates the cumulative probability joined to the Weibull distribution F(δ_{550}) and the measurement data histogram.

Finally, In order to be able to use the Weibull distribution and to validate it the statistical test of Kolmogorov Smirnov can be adopted. So the parameter, representing the Kolmogorov-Smirnov test (ks), is computed through the following expression:

$$ks = Max\left|F(\delta_{550}) - \hat{F}(\delta_{550})\right| \qquad (2)$$

The likelihood of the presence of initial rejection, defined by the significance level for ks equal to 10% the critical parameters for the significance level are evaluated (in the analogue process for wind speed data analysis).

$$ks_{10}(n) = 0.8324905 - 0.199103 \cdot n^{-\frac{1}{2}} \qquad (3)$$

$$ks_{10}(n) = 0.026511 \cdot ks + 0.002725911 \cdot ks^{2} \qquad (4)$$

The parameter ks* for the number of "n" bins of the AOD histograms is given by:

$$ks^{*} = ks \cdot n^{\frac{1}{2}} \qquad (5)$$

If the value of ks* is greater than the value of the critical parameter ks_{10}, then the used method is not adequate for the specific AOD data.

In the point of view of tailed distribution, the weibull distribution having β greater than 1 is defined as a light-tailed distribution, [39], in the converse case, a coefficient of variation having lower value is determined and used to test adequation weibull with heavy tailed:

$$CVI_{\delta 550} = \frac{\sigma}{\langle \delta_{550} \rangle} = \sqrt{\left(\frac{\Gamma(1+\frac{2}{\beta})}{\Gamma^2(1+\frac{1}{\beta})} - 1 \right)} \qquad (6)$$

Also the coefficient of variation index, (CVI) [40] designate a value close to 1 (or 100 %) signifies a model equivalent to the measured data, a value less than 1 a better model, and a value greater than 1, an undesired model.

2.3. Moroccan Location of the Studied Sites

In order to carry out our study, the data for various specific locations (mountainous, desert, valleys, prairies and littoral areas), altitudes (high and low level) and climates were selected. Figure 2 shows the following sites:
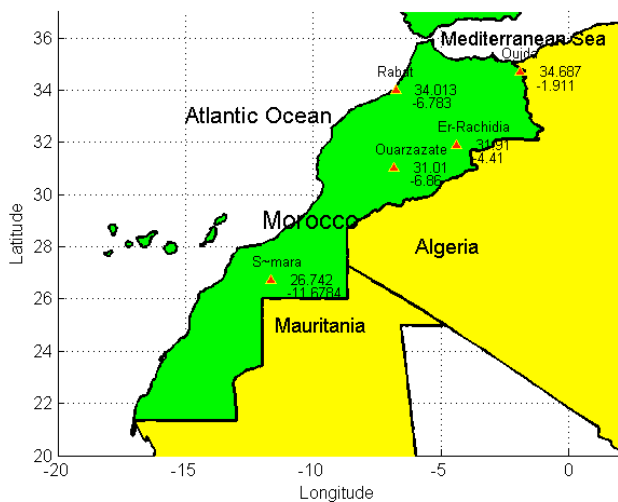

Fig. 2. Morocco / Rabat, Oujda, Ouarzazate, Er-Rachidia and S'mara location sites.

➢ Oujda, latitude 34.687, longitude -1.911, altitude 650 m agl, area with predominance climate under both Mediterranean and continental influence.

➢ Rabat, latitude 34.013, longitude - 6.783, altitude 114m agl, littoral area with oceanic influence.

➢ Er-rachidia, latitude 31.910, longitude -4.410, altitude 1029 m agl, desert and arid environment influenced by the continental climate,

➢ S'mara, latitude 26.742, longitude -11.6784, altitude 287 m agl, desert-saharien climate at 220 km far from the oceanic littoral.

➢ Ouarzazate, latitude 31.010, longitude -6.860, altitude 1543 m agl, arid climate under mountain shadow and continental influence.

2.4. Meteorological Data

The Modern-Era Retrospective analysis for Research and Applications, (MERRA DATA) free web service, available on the internet, delivers time series of temperature at 2 m above ground level (agl), relative humidity (at 2 m agl), pressure (at 2m agl), wind speed and direction (at 10 m agl), rainfall, snowfall and snow depth.

The data range time step is hourly. The spatial resolution approximately is 50 km. The data are extracted since Jan 2005 up to Dec 2015, followed by the controlling process for the quality of measurements of meteorological data (QCP), based on variables extrema, and maxima step for two measures are verified [41].

2.5. Aerosol Data Processing

Aerosol Optical Depth (AOD) data used in this paper come from MACC reanalysis aerosol, by intermediate The CAMS-AOD under grant agreement no. 218793 (MACC project, 2009-2011), no. 283576 (MACC-II EU-funded project, 2011-2014), which is a free service available on the internet, delivers time series of aerosols provided, the time coverage of the data is from 2005-01-01 up to 2015-12-07. Time step is 3 hours. The Aerosol Optical Depth measured at wavelength of 550 nm and 1240 nm, concerned the total AOD, Black Carbon, Dust, Organic Mater, Sea Salt and Sulfate.

3. Results and Discussions

Figure 3 (a) shows AOD data of 11 years at 550 nm, and (b) the Angstrom exponent known as the fine mode fraction (FMF) variation. We observe the atmospheric AOD behavior change from January 2013. A sample of 31936 points is tri-hourly bearings from of AOD (a). The variations of aerosol optical depth and the fine mode fraction are presented. The values of δ_{550} varying during the period from 2005 up to 2012 (period: P1) are quasi stable in the majority of sites, ranging between of 0 and 0.8, the FMF making a band from #0.85 to 1.5
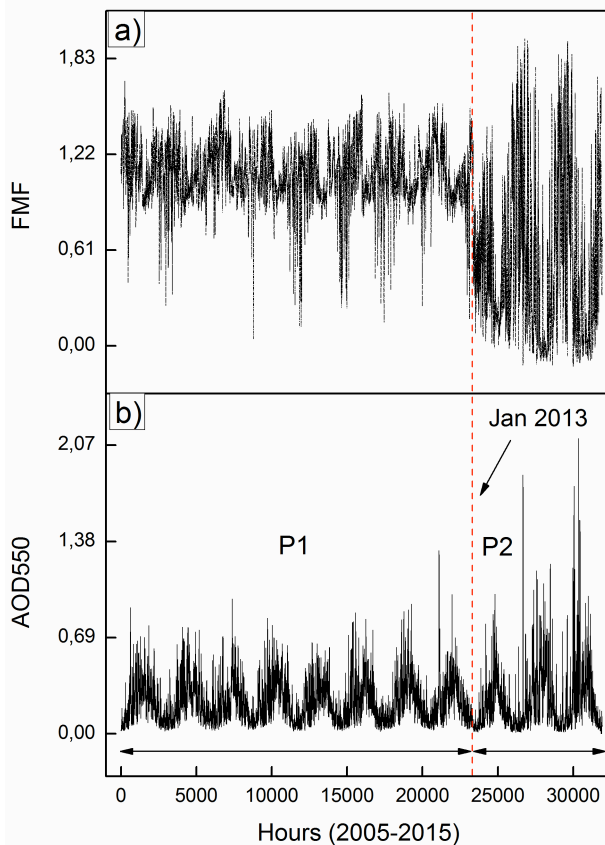
Fig. 3. Aerosol Optical Depth at wavelength 550 nm measurement from Jan. 01 2005 up to Dec. 06 2015 hourly averaged for Ouarzazate location, (may be the same for the others location) (a) Fine mode fraction data, (b) Time-series data.

However during the period 2013 up to 2015 (P2), the FMF indicate that the atmosphere is more turbid, decreasing from January with lower than one until the minimum reached to 0 after increasing to 1.75; while the rainfall during P1 is regular than P2, so the atmosphere is more turbid by the AOD during P2 than P1 because, it is not sufficiently cleaned, from particles subsisted there; some crystal water particles are added, and/or coarse aerosols established. A low value of FMF describes more coarse particles exist in the atmosphere and vice versa, due to a relationship between the FMF and a rainfall.

Morocco is a country rich with its various variables climates, Rabat as an Atlantic location and Oujda as a Mediterranean location, have the same particularity as they are near the sea. Furthermore, the anthropic particles coming from industrial activities, in addition for Oujda where the continental dust come to participate for disturbing atmosphere; the rainfall were not heavy during P2 in comparison to P1, S'mara a desert region, where the continental dust is very abundant, somewhere the lightly rainfall is the behavior of the site. In the inference, the AOD variation needs to be statistically analyzed in each region, during the rainy and dry periods.

Figure 4 displays the evolution of rainfall and fine mode fraction during both the periods. The regions that are under the continental influence (Ouarzazate, Oujda and Er-Rachidia) where the same rainfall disturbance reigned during the period P2, than the period P1. Thus the FMF possess lower values with a high variability, which means that the atmosphere in these regions contains coarse aerosols; while the region of S'mara is known to have desert climate from where the rainfall is mostly low. On the other hand, the Rabat region under the oceanic influence takes an intermediate status due to the presence of relative humidity, high temperature and sea salt.
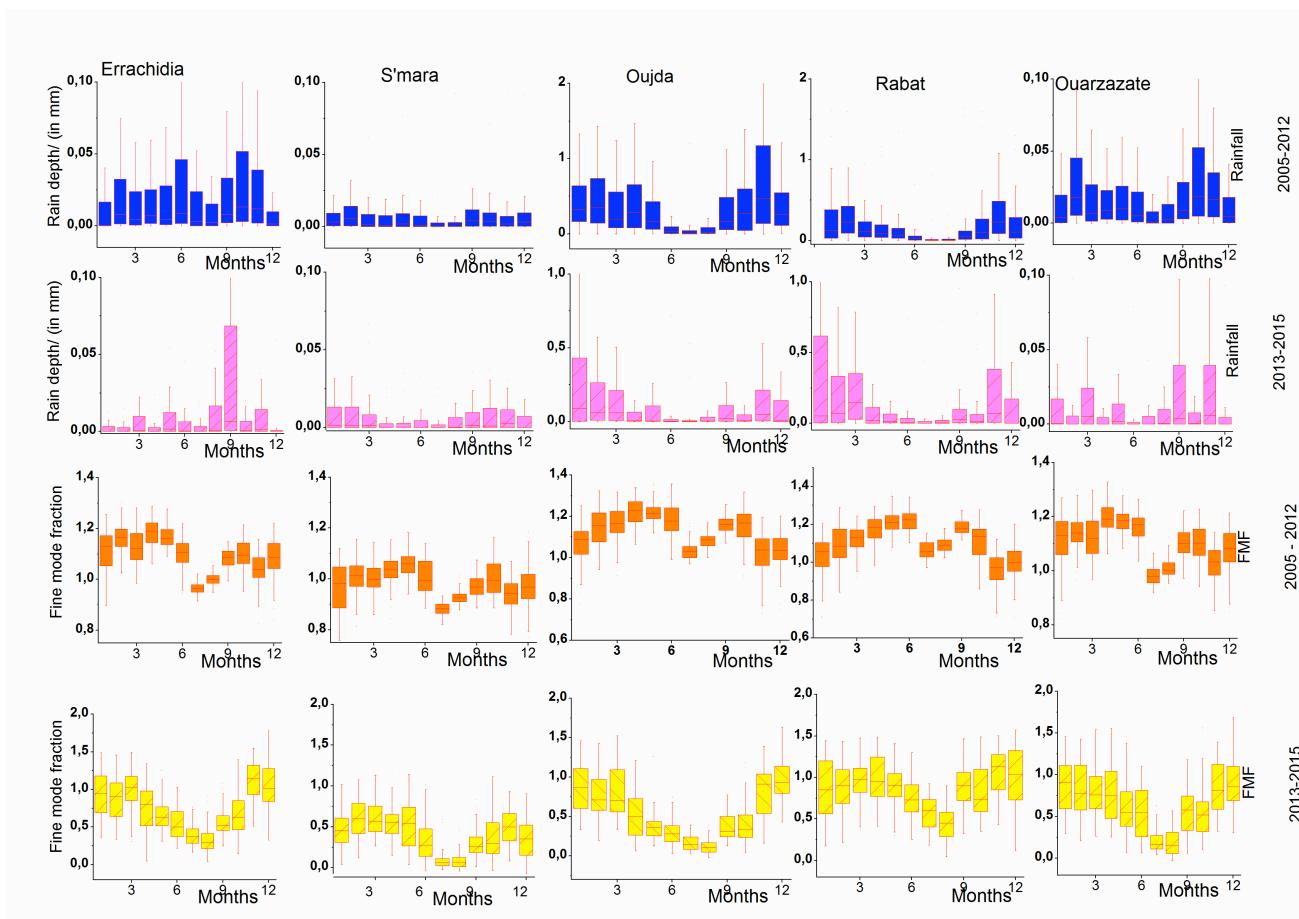
Fig. 4. Annually boxplot variation of the fine mode fraction and rain depth related to location under study

Figures 5 and 6 illustrate for each month, the cumulative distribution function of the Weibull distribution plotted against the cumulative frequency distribution of measured. These curves illustrate the Weibull methods that fit best to the measured AOD data.

The *ks* test results are summarized in table 1. The goodness of fit tests summarized in (subplot (a) is related to the period P1 and subplot (b) is related to the–period P2), show that the *ks** is higher than the critical value ks.$_{10}$ in all case studied by month, so any interval data does not rejected by the Kolmogorov-Smirnov test. Likewise, the Maximum Likelihood in our case studied has been proved adequate for the available AOD data from for the two times scales data conditions P1 and P2. As a result, the weibull distribution model is validated for predicting Aerosol Optical Depth. But the form parameter β is less than 1 in February for all locations excluding S'mara, a pure desert area. This conditions describes that the distribution can be ranked as heavy-tailed [33], therefore the same case can be modeled by log-normal distribution.

In the case of irregular rainy season in winter (February) in P2, the variation of AOD in the atmosphere is not steady (as discussed above). The coefficient of variation index is very large describing in fact the atmosphere. The form parameter is less than one and the distribution shows flatness. Therefore, the form parameter depends on the state of the weather at certain location. Table 1 (Annex) illustrate

the monthly averaged AOD and their variability CVI for all the sites, and show that during the period P1, the variability is around 0.5 with a minimum less than 0.261 in august and a maximum up to 0.617 (the both extrema registries in Er-Rachidia region). Whereas, during the period P2 where the variability of AOD is much dispersed, the CVI is greater than 1 in February during the winter season except for S'mara which keeps the same behavior as the period P1. This may justify that why the regularity of the rain gives stability for the atmosphere. The low value of the variability confirms that the reliability of the approximation of the CDF to measurements distribution is true when the climate is regular. The coefficient of variation index CVI is very low which makes it worth perceiving that the weibull distribution is a suitable model to model AOD data. Therefore, in our cases the log-normal results are equivalent to those calculated by weibull model.
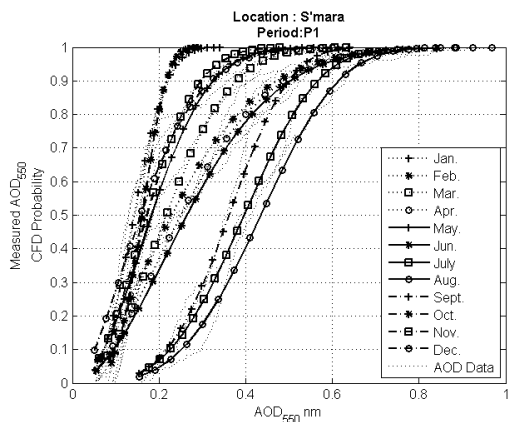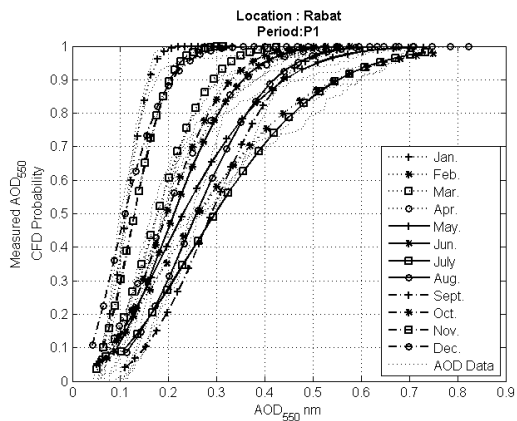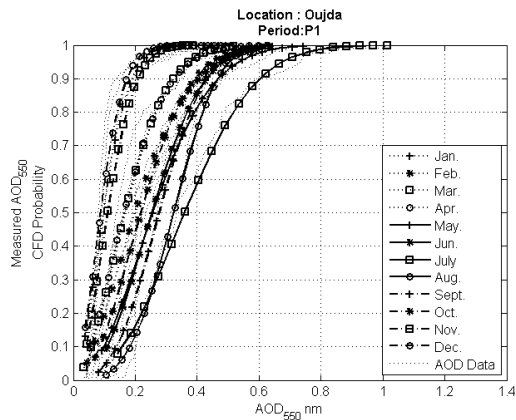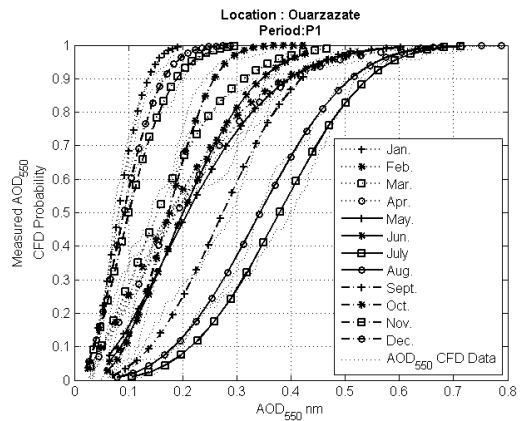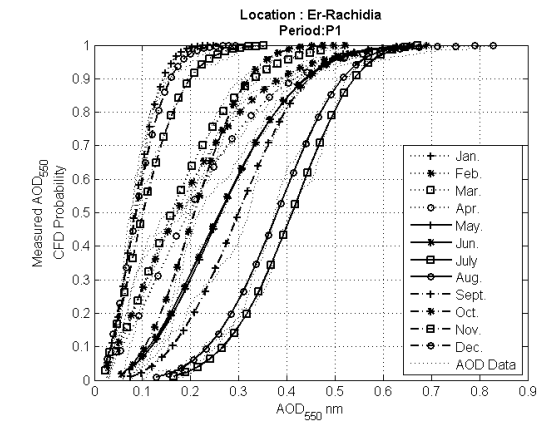
Fig. 5. AOD_{550} Cumulative Distribution Function Data and its monthly goodness of fit during period P1:2005-2012
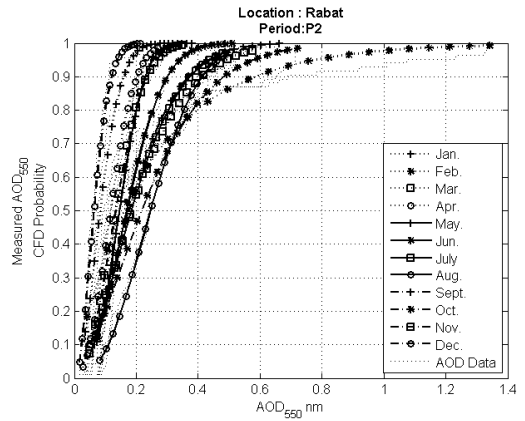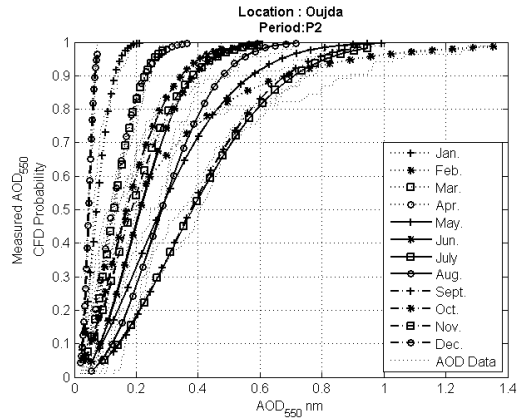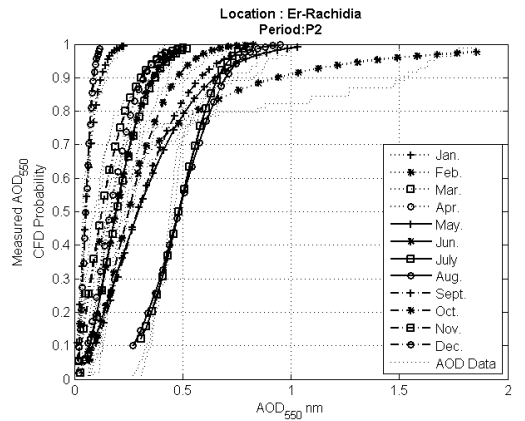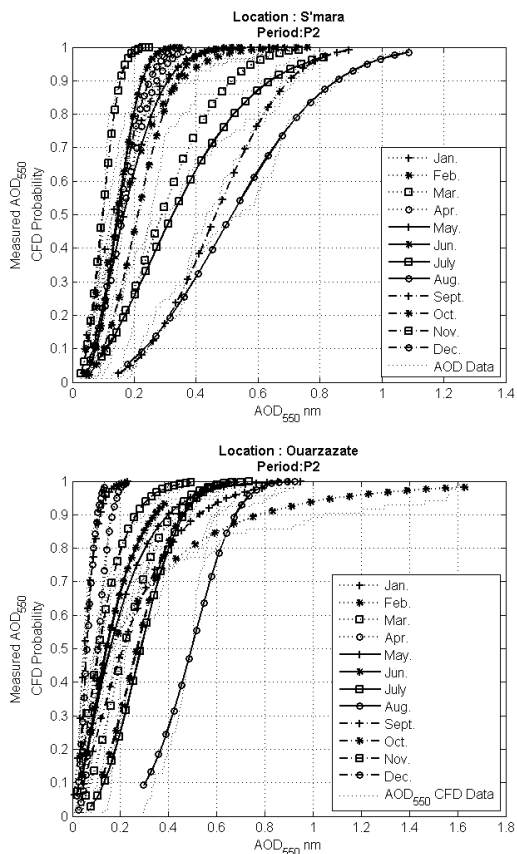
Fig. 6. AOD$_{550}$ Cumulative Distribution Function Data and its monthly goodness of fit during period P1:2005-2012.

Since the scale and the shape parameters were determined using the maximum likelihood method as the estimation method, we can associate the averaged AOD by gamma function, with the statistical average of the water vapor atmospheric column content, as it is presented in the new formulation of Ineichen. Therefore, the factor of Linke can be determined easily, and the coefficient of atmospheric attenuation relative to the radiation reflected from the heliostat to the tower receiver according to the Polo formula, for an average distance of 1.3 Km. Table 1 displays attenuations relative to each and every site. The series of T_L achieved are reported in the same table (Annex) and plotted in figures. 8 and 9.

Figure 10 shows that the Moroccan regions are heterogeneous and can therefore be classified into two groups according to the values of AOD averaged and their variations throughout the year.

Four curves related to the northern regions of Morocco are analogous, revealing the AOD variations are the same throughout the year during heavy rainfall period (P1) as displayed in figure 10.
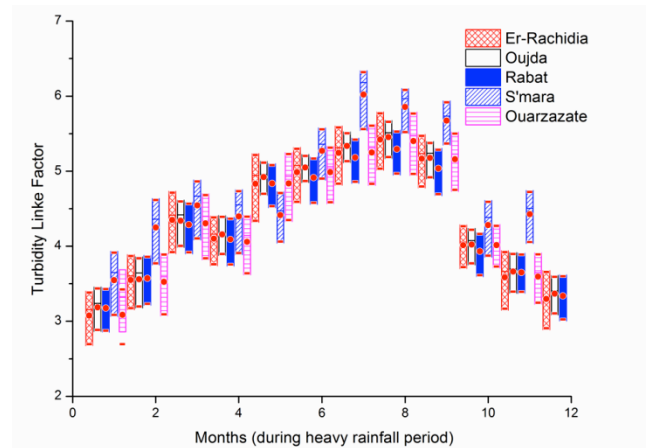
Fig. 8. Turbidity Linke factor during P1: heavy rainfall period
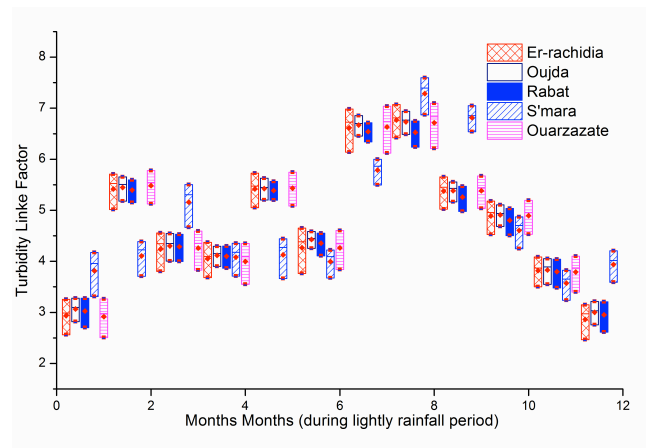
Fig.9. Turbidity Linke factor during P2: lightly rainfall period

Figures 11-15, shows the AOD averaged variation with standard deviation errors for each case and locations separately wherein, errors are very small in the period P1 than P2. The standard deviation has been estimated by employing weibull distribution parameters [42].
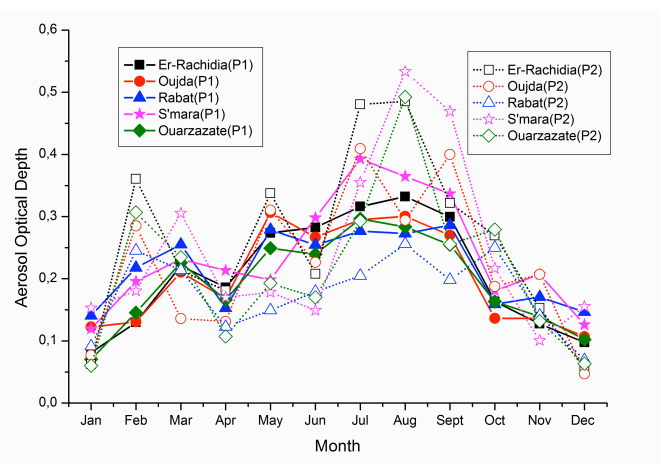
Fig.10. AOD$_{550}$ during period (1 and 2) in the compared sites.
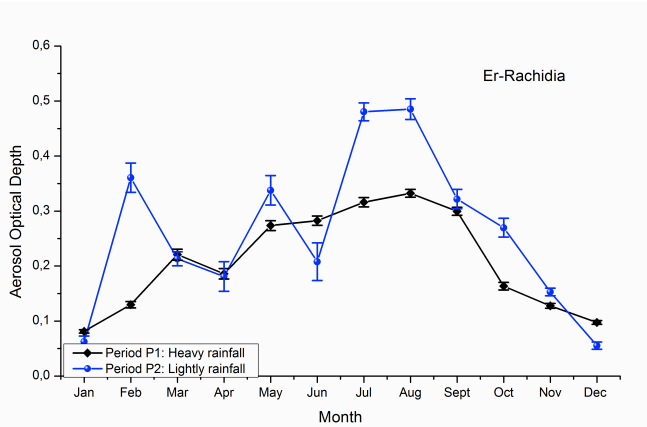
Fig.11. AOD$_{550}$ in Er-Rachidia during the compared Periods
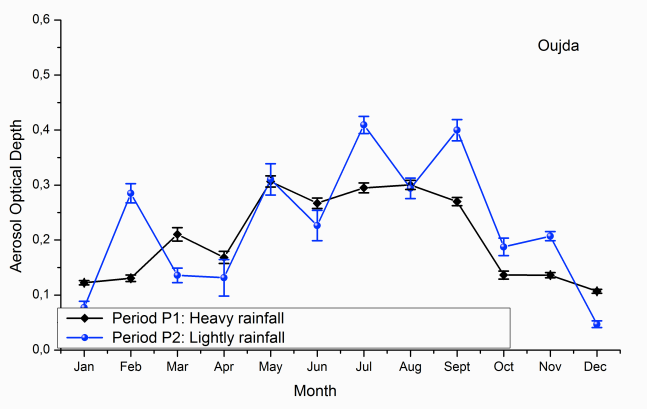
Fig.12. AOD$_{550}$ in Oujda during the compared Periods

These groups are related to the following climate groups:

➢ G1: northern Group characterized globally by littoral locations with low altitude (Rabat, Oujda), and in the desert locations with high altitude (Ouarzazate, Er-rachidia) where climate is under mountain shadow, giving moderate atmospheric water atmospheric vapor content, aerosols optical depth (the whole year have less than 0.3).

➢ G2 (S'mara): Southern Group characterized by their desert climate, having dust as aerosols reign (quarter year with AOD greater than 0.3) with low atmospheric water vapor and low altitude.

The group G1 includes zones with high altitude maximum more than 1500 m above sea level (ASL); desert climate under mountain climate effect causes partly humid atmosphere, and the minimum Rabat (114m ASL) located near the oceanic Atlantic and the medium altitude (more than 600 m) located near the Mediterranean's sea cold semi-arid

climate (Oujda).
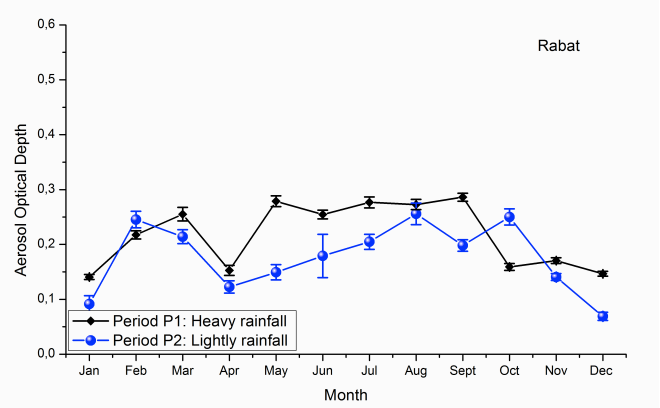
Fig.13. AOD$_{550}$ in Rabat during the compared Periods
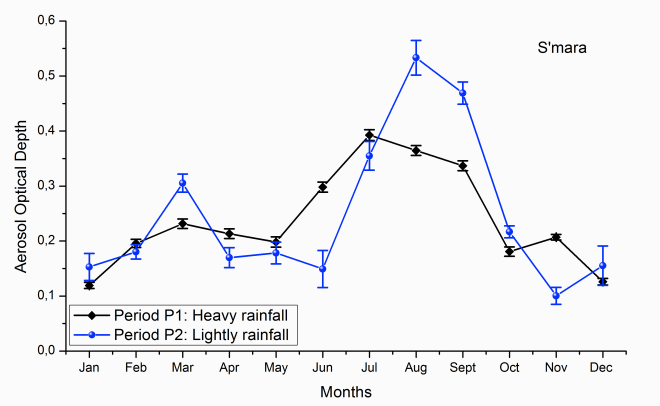
Fig.14. AOD$_{550}$ in S'mara during the compared Periods
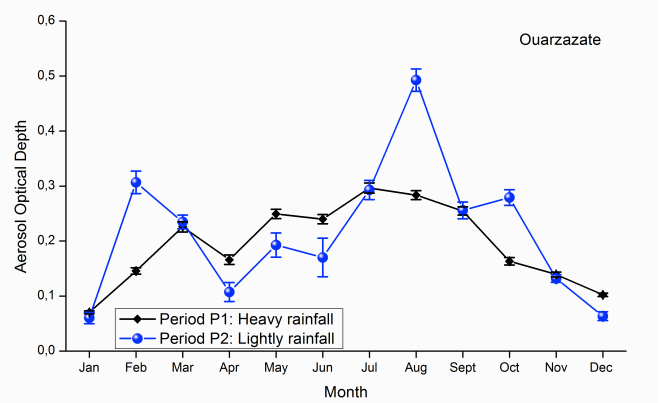
Fig.15. AOD$_{550}$ in Ouarzazate during the compared Periods

Therefore, the altitude and water vapor contents do not have a noticeable impact on the atmosphere turbidity.

The southern group G2 includes the desert climate with low altitudes wherein the dust/sand are major elements transported by the wind (S'mara location).

The two zones are in accordance with both the aerosols and water vapors demonstrate the same variation which is dependent on the climatic and geographical conditions. Humidity along with sand and dust transported by winds consequently makes the T_L factor high, fluctuating around 3.5 (highest 5.5 in august in Oujda and the lowest 3.13 in January in Ouarzazate). Not so far from this group AOD

ranking, we found in (Rabat), lower altitude, introduces a warm-summer climate near the Atlantic ocean with a predominance of humidity where sea salt thickness increase with temperature growing.

Group G2 S'mara which is almost 200 km from the ocean with lower altitude: The T_L is sensitively greater than the others regions and fluctuates around 4.5 with lower values in winter in January (3.6) and the highest values in July (reach to 6).

Fig 9 shows an evolution of the Turbidity Linke factor which fluctuates considerably during a long period (winter, spring and summer seasons). This state of the atmosphere is hard to judge, and assesses the key indicators of solar extinction.

Under the climatological regularity, it can be inferred that the turbidity Linke factor demonstrates a regular increases until a maximum in July and then decreases in a similar way until December; whereas it is unstable in the converse case.

The third polynomial coefficients of the equation of atmospheric attenuation slant in the solar tower project are shown in table 1 (Annex). The results depict that in the solar tower plant, the atmospheric attenuation for the slant path for an average distance of 1.3 Km on the irregular rainfall period can reach 28% at Er-Rachidia (February) and the lower in Oujda (December) with 3.3%, but in the regular rainfall period. The attenuation is though very steady and oscillates between 3% and 15.9%.

The atmospheric attenuation for solar tower power plant can reach 28% at Er-rachidia (February) and 26% at S'mara (August) and fluctuate around 11% in the others cases locations and regular rainfall period.

4. Conclusion

Aiming at optimal management [43,44] and sizing of energy systems installation using solar tower technology, the tri-hourly Aerosol Optical Depth data format have been statistically analyzed in two timescales conditions, a regular rainfall period and an irregular one. Based on the fine mode fraction classification, the qualification periods were considered for the Moroccan location refereeing to various climate dominance for each region under oceanic effect Mediterranean, continental, desert, Sahara and mountain influence.

Thus, the most significant outcomes of this work can be summarized as following:

➤ Aerosol Optical Depth described by Weibull probability function. The scale parameter α and shape parameter β which are summarized in table 1.

➤ The Kolmogorov smirnov ks test and the coefficient of variation index CVI validate the selected weibull PDF for describing the atmospheric AOD behaviours in two timescales conditions; in the various climates of Morocco, which can be accomplished on an atlas of AOD.

➤ Using the new formulation of Ineichen, the turbidity Linke factor can be estimated by using the averaged δ_{550} assessed previously besides the atmospheric water vapor easily available are presented in table 1 (Annex).

➤ The Linke turbidity factor related to the attenuation up to top of atmosphere were estimated from $T_L=3$ on the winter season and grow straight to $T_L=6$ on the summer season in the regular rainfall period; it fluctuates between 3 and 6 in the other period. It can also be noted that S'mara has steady low attenuation coefficient in two periods because this region is known for light rainfall.

➤ The atmospheric attenuation for solar tower power plant estimated 11 % on the regular rainfall period.

Initially tested on Moroccan regions, this approach can be generalized on regions with similar climatic conditions. This approach might also find applications in renewable energy, specifically in the field solar tower technology.

Acknowledgements

References

[1] F. Mavromatakis and Y. Franghiadakis. Direct and indirect determination of the linke turbidity coefficient. Solar Energy, 81(7):896–903, jul 2007.

[2] Yousef A. Eltbaakh, M.H. Ruslan, M.A. Alghoul, M.Y. Othman, K. Sopian, and T.M. Razykov. Solar attenuation by aerosols: An overview. Renewable and Sustainable Energy Reviews, 16(6):4264–4276, aug 2012.

[3] R MUELLER. Rethinking satellite-based solar irradiance modellingThe SOLIS clear-sky module. Remote Sensing of Environment, 91(2):160–174, may 2004.

[4] A. Trabelsi and M. Masmoudi. An investigation of atmospheric turbidity over kerkennah island in tunisia. Atmospheric Research, 101(1-2):22–30, jul 2011.

[5] Bo Leckner. The spectral distribution of solar radiation at the earths surfaceelements of a model. Solar Energy, 20(2):143–150, 1978.

[6] David, A., Joseph, E., Ngwa, N. R., & Arreyndip, N. A. (2018). Global Solar Radiation of some Regions of Cameroon using the Linear Angstrom Model and Non-linear Polynomial Relations: Part 2, Sun-path Diagrams, Energy Potential Predictions and Statistical Validation. International Journal of Renewable Energy Research (IJRER), 8(1), 649-660.

[7] Yesilbudak, M., Colak, M., & Bayindir, R. (2018). What are the Current Status and Future Prospects in Solar Irradiance and Solar Power Forecasting? International Journal of Renewable Energy Research (IJRER), 8(1), 635-648.S

[8] Harrouni, S and Maafi, A. Classification des éclairements solaires à l'aide de l'analyse fractale. Revue Internationale des éenergies renouvelables, 5:107–122, 2002.

[9] A Maafi and S Harrouni. Measuring the fractal dimension of solar irradiance in view of pv systems performance analysis. In World Renewable Energy Congress VI, pages 2032–2035. Elsevier, 2000.

[10] M. Yilmaz, B. Gumus, H. Kilic et M. E. Asker, Chaotic analysis of the gloabal solar irradiance, chez 2017 {IEEE} 6th International Conference on Renewable Energy Research and Applications (ICRERA), 2017.

[11] A Sfetsos and AH Coonick. Univariate and multivariate forecasting of hourly solar radiation with artificial intelligence techniques. Solar Energy, 68(2):169–178, 2000.

[12] S Barbaro, G Cannata, S Coppolino, C Leone, and E Sinagra. Correlation between relative sunshine and state of the sky. Solar Energy, 26(6):537–550, 1981.

[13] J Cañada. Global solar radiation in pais valenciano using sunshine hours. International journal of ambient energy, 9(4):197–202, 1988.

[14] Christian Gueymard. Analysis of monthly average solar radiation and bright sunshine for different thresholds at cape canaveral, florida. Solar Energy, 51(2):139–145, 1993.

[15] I. Supit and R.R. van Kappel. A simple method to estimate global radiation. Solar Energy, 63(3):147–160, sep 1998.

[16] B. Tammelin, T. Vihma, Production of the Finnish Wind Atlas, Wind Energy, vol. 16, pp. 19-35, 12 2011.

[17] S. AlYahya et M. A. Irfan, New solar radiation Atlas for Saudi Arabia, chez 2014 International Conference on Renewable Energy Research and Application (ICRERA), 2014.

[18] I. Razika, I. Nabila et M. Marouane, Comparison between hybrid Weibull and MEP methods for calculating wind speed distribution, chez 2014 5th International Renewable Energy Congress (IREC), 2014.

[19] A.N. Alias, M.Z. MatJafri, H.S. Lim, N.M. Saleh, S.H. Chumiran, and A. Mohamad. Inferring angstrom exponent and aerosol optical depth from AERONET. Journal of Environmental Science and Technology, mar 2014.

[20] Pierre Ineichen. A broadband simplified version of the solis clear sky model. Solar Energy, aug 2008.

[21] Pierre Ineichen. Conversion function between the linke turbidity and the atmospheric water vapor and aerosol content. Solar Energy, 82(11):1095–1097, nov 2008.

[22] Natalie Hanrieder, Stefan Wilbert, Marion Schroedter-Homscheidt, Franziska Schnell, Diana Mancera Guevara, Reiner Buck, Stefano Giuliano, and Robert Pitz-Paal. Atmospheric extinction in simulation tools for solar tower plants. Author(s), 2017.

[23] Jesús Polo, Jesús Ballestrn, and Elena Carra. Sensitivity study for modelling atmospheric attenuation of solar radiation with radiative transfer models and the impact in solar tower plant production. Solar Energy, sep 2016.

[24] Abdelouahid Tahiri, Mohammed Diouri, Hanae Steli, Ibtissam Marsli, Rajae Meziane, and Abdelmoula Bentayeb. Desert aerosol optical properties in morocco. Environmental Sciences, 4:63–78, 2016.

[25] N. Hanrieder, M. Sengupta, Y. Xie, S. Wilbert, and R. Pitz-Paal. Modeling beam attenuation in solar tower plants using common DNI measurements. Solar Energy, 129:244–255, may 2016.

[26] F Wagner and AM Silva. Some considerations about ångström exponent distributions. Atmospheric Chemistry and Physics, 8(3):481–489, 2008.

[27] K. C. Kaku, J. S. Reid, N. T. ONeill, P. K. Quinn, D. J. Coffman, and T. F. Eck. Verification and application of the extended spectral deconvolution algorithm (SDA) methodology to estimate aerosol fine and coarse mode extinction coefficients in the marine boundary layer. Atmospheric Measurement Techniques, oct 2014.

[28] V Matthias. The aerosol distribution in europe derived with the community multiscale air quality (cmaq) model: comparison to near surface in situ and sunphotometer measurements. Atmospheric Chemistry and Physics, 8(17):5077–5097, 2008.

[29] Mian Chin, Allen Chu, Robert Levy, Lorraine Remer, Yoram Kaufman, Brent Holben, Tom Eck, Paul Ginoux, and Qingxian Gao. Aerosol distribution in the northern hemisphere during ace-asia: Results from global model, satellite observations, and sun photometer

measurements. Journal of Geophysical Research: Atmospheres, 109(D23), 2004.

[30] Mikhail D Alexandrov, Alexander Marshak, Brian Cairns, Andrew A Lacis, and Barbara E Carlson. Scaling properties of aerosol optical thickness retrieved from ground-based measurements. Journal of the atmospheric sciences, 61(9):1024–1039, 2004.

[31] James Foster, Michael Bevis, and William Raymond. Precipitable water and the lognormal distribution. Journal of Geophysical Research: Atmospheres, 111(D15), 2006.

[32] Youfei Zheng, Jianjun Liu, Rongjun Wu, Zhanqing Li, Biao Wang, and Takamura Tamio. Seasonal statistical characteristics of aerosol optical properties at a site near a dust region in china. Journal of Geophysical Research: Atmospheres, 113(D16), 2008.

[33] Oleg Dubovik, Brent Holben, Thomas F Eck, Alexander Smirnov, Yoram J Kaufman, Michael D King, Didier Tanré, and Ilya Slutsker. Variability of absorption and optical properties of key aerosol types observed in worldwide locations. Journal of the atmospheric sciences, 59(3):590–608, 2002.

[34] J Cermak and Reto Knutti. Beijing olympics as an aerosol field experiment. Geophysical Research Letters, 36(10), 2009.

[35] O'Neill N. T., A. Ignatov, B. N. Holben, and T. F. Eck. The lognormal distribution as a reference for reporting aerosol optical depth statistics empirical tests using multi-year, multi-site AERONET sunphotometer data. Geophysical Research Letters, 27(20):3333–3336, oct 2000.

[36] Yang Liu, Jeremy A Sarnat, Brent A Coull, Petros Koutrakis, and Daniel J Jacob. Validation of multiangle imaging spectroradiometer (misr) aerosol optical thickness measurements using aerosol robotic network (aeronet) observations over the contiguous united states.

Journal of Geophysical Research: Atmospheres, 109(D6), 2004.

[37] Wu Lin and Zeng Qing-Cun. Study on probability distributions of multi-timescale aerosol optical depth using AERONET data. Atmospheric and Oceanic Science Letters, 4(4):216–222, jan 2011.

[38] Ahmed Ouammi, Valeria Ghigliotti, Michela Robba, Abdelaziz Mimet, and Roberto Sacile. A decision support system for the optimal exploitation of wind energy on regional scale. Renewable Energy, 37(1):299–309, jan 2012.

[39] Michael Mitzenmacher. A brief history of generative models for power law and lognormal distributions. Internet mathematics, 1(2):226–251, 2004.

[40] Alma Riska. Aggregate matrix-analytic techniques and their applications. 2002.

[41] M. Geiger, L. Diabaté, L. Ménard, and L. Wald. A web service for controlling the quality of measurements of global solar irradiation. Solar Energy, 73(6):475–480, dec 2002.

[42] F.B. Amar, M. Elamouri. A New theoretical model for modeling the wind speed frequency distribution. International Journal of Renewable Energy Research, 1(4):306-313, 2012.

[43] S. Han et H. W. Shin, «Policy trends of renewable energy in Korea,» chez 2014 International Conference on Renewable Energy Research and Application (ICRERA), 2014.

[44] F. Viola, P. Romano, R. Miceli, D. L. Cascia, M. Longo et G. Sauba, Economical evaluation of ecological benefits of the demand side management, chez 2014 International Conference on Renewable Energy Research and Application (ICRERA), 2014.

Annex

Table 1: Komogorov test validation result, the inferred weibull parameters, Linke turbidity factor, the heliostat attenuation atmosphere, and the parameters of the attenuation loss between the heliostat and the solar receiver (Left: P1; Right: P2)

Er-Rachidia

P2: Lightly rainfall (S=1.3 Km)

Month	Ks	Ks.10	Ks*	α	β	<AOD(P2)>	p3	p2	p1	p0	A(%)	wp(cm)	TL
1	0.158	0.004	0.038	0.068	1.366	0.077	-0.19	3.38	3.27	0.04	4.016	0.85	3.152
2	0.239	0.007	0.058	0.287	0.706	0.361	-15.02	38.51	28.202	-1.46	5.526	0.94	3.603
3	0.088	0.002	0.021	0.153	1.886	0.213	2.12	2.12	10.654	-0.22	4.347	1.04	4.414
4	0.193	0.005	0.047	0.204	1.833	0.181	0.11	1.68	9.218	-0.37	4.097	1.16	4.162
5	0.102	0.003	0.025	0.181	1.511	0.338	0.41	4.57	18.50	-0.21	4.383	1.27	4.943
6	0.123	0.003	0.030	0.374	1.680	0.310	0.32	6.73	16.853	-0.33	4.153	1.48	5.075
7	0.131	0.004	0.031	0.234	1.893	0.208	0.17	2.05	10.420	-0.21	4.383	1.30	5.313
8	0.210	0.006	0.051	0.532	3.761	0.480	0.53	6.59	23.224	-0.53	6.727	1.36	5.734
9	0.186	0.005	0.045	0.541	3.257	0.485	0.61	6.82	25.85	-0.53	6.810	1.54	5.234
10	0.120	0.003	0.038	0.361	1.733	0.322	0.34	4.02	17.11	-0.35	5.454	1.46	4.055
11	0.149	0.004	0.029	0.304	1.876	0.270	0.24	3.01	13.93	-0.29	4.956	1.16	3.662
12	0.096	0.003	0.036	0.167	1.353	0.153	-0.04	1.34	7.87	-0.12	3.868	0.95	3.33

Oujda

Month	Ks	Ks.10	Ks*	α	β	<AOD(P2)>	p3	p2	p1	p0	A(%)	wp(cm)	TL
1	0.140	0.004	0.034	0.272	2.086	0.285	-0.36	4.10	15.657	-0.37	3.919	1.36	3.644
2	0.163	0.004	0.039	0.153	0.909	0.136	-0.53	4.78	13.094	-0.11	5.441	1.35	3.628
3	0.193	0.005	0.047	0.148	2.086	0.131	3.66	17.96	10.767	-0.37	5.508	1.49	4.419
4	0.165	0.004	0.040	0.255	1.940	0.310	2.22	5.02	7.029	-0.10	4.350	1.51	4.378
5	0.112	0.003	0.027	0.348	1.680	0.226	1.02	6.73	7.804	-0.08	4.133	1.64	4.150
6	0.070	0.002	0.017	0.007	2.007	0.179	0.07	1.23	9.120	-0.13	4.404	1.78	4.187
7	0.105	0.003	0.025	0.461	1.933	0.409	0.52	22.52	20.226	-0.46	6.702	2.02	4.957
8	0.128	0.003	0.031	0.332	2.267	0.294	0.27	3.32	14.335	-0.32	6.766	2.30	5.076
9	0.072	0.002	0.017	0.221	2.015	0.198	0.14	1.94	10.14	-0.19	5.429	2.46	5.127
10	0.197	0.005	0.047	0.451	1.669	0.400	0.22	2.82	10.005	-0.25	4.940	2.11	5.239
11	0.121	0.003	0.035	0.232	1.653	0.207	0.06	1.13	10.61	-0.11	5.682	2.08	4.075
12	0.108	0.003	0.026	0.062	3.378	0.055	-0.05	0.11	3.04	0.05	3.713	1.13	3.662

Rabat

S=1.3 Km

Month	Ks	Ks.10	Ks*	α	β	<AOD(P2)>	p3	p2	p1	p0	A(%)	wp(cm)	TL
1	0.137	0.004	0.033	0.087	1.897	0.091	-0.53	1.33	7.84	-0.03	5.281	1.50	3.099
2	0.197	0.005	0.047	0.236	0.921	0.245	0.35	1.71	9.26	-0.16	5.526	1.49	3.644
3	0.221	0.006	0.053	0.237	1.506	0.305	0.29	3.55	15.85	-0.33	5.305	1.73	4.337
4	0.098	0.003	0.024	0.192	2.338	0.170	0.10	1.50	8.61	-0.16	4.176	1.96	4.133
5	0.203	0.005	0.049	0.201	1.952	0.178	0.11	1.63	9.06	-0.17	4.273	1.85	5.394
6	0.063	0.002	0.015	0.168	2.813	0.149	0.07	1.23	7.59	-0.13	4.091	2.13	4.404
7	0.123	0.003	0.030	0.399	1.760	0.355	0.41	4.69	19.17	-0.39	5.865	2.27	5.000
8	0.089	0.002	0.021	0.602	2.393	0.533	0.83	8.57	30.78	-0.61	7.393	2.40	6.180
9	0.097	0.003	0.023	0.526	2.912	0.469	0.59	6.56	25.51	-0.52	6.855	2.55	5.965
10	0.107	0.003	0.026	0.244	2.583	0.217	0.15	2.12	10.96	-0.23	4.703	2.58	5.734
11	0.126	0.005	0.030	0.277	1.491	0.250	0.22	2.82	13.08	-0.25	4.867	2.37	5.127
12	0.127	0.003	0.030	0.159	2.123	0.100	0.01	0.64	5.22	-0.05	10.781	2.05	4.703

S'mara

Month	Ks	Ks.10	Ks*	α	β	<AOD(P2)>	p3	p2	p1	p0	A(%)	wp(cm)	TL
1	0.123	0.003	0.026	0.052	1.904	0.069	-0.06	0.27	3.71	0.02	8.069	1.74	3.867
12	...	...	...	...	...	...	-0.03	1.13	7.18	-0.11	4.311	1.47	3.036

Ouarzazate

Month	Ks	Ks.10	Ks*	α	β	<AOD(P2)>	p3	p2	p1	p0	A(%)	wp(cm)	TL
1	0.170	0.004	0.041	0.066	1.467	0.060	-0.05	0.16	3.27	0.04	2.979	0.79	3.648
2	0.196	0.005	0.047	0.261	0.764	0.307	1.05	8.11	24.24	-0.67	5.545	0.78	3.593
3	0.127	0.003	0.030	0.264	1.822	0.235	0.18	2.46	12.02	-0.24	5.465	0.97	4.397
4	0.086	0.004	0.021	0.121	2.633	0.107	0.02	0.72	5.55	-0.06	5.975	1.00	4.089
5	0.161	0.004	0.039	0.208	1.273	0.193	0.10	1.97	10.03	-0.17	9.845	1.07	4.551
6	0.205	0.006	0.049	0.186	1.369	0.170	0.14	1.59	8.75	-0.14	8.773	1.06	5.059
7	0.096	0.003	0.023	0.330	2.461	0.293	0.26	3.26	15.00	-0.32	14.253	1.29	5.372
8	0.168	0.005	0.040	0.545	3.817	0.493	0.61	6.85	26.63	-0.54	23.848	1.23	5.473
9	0.142	0.004	0.034	0.287	1.291	0.256	0.25	3.08	13.69	-0.26	12.879	1.36	5.227
10	0.141	0.004	0.315	0.315	2.248	0.279	0.24	3.08	14.31	-0.30	13.640	1.32	4.942
11	0.113	0.003	0.027	0.144	1.367	0.132	0.05	1.06	6.80	-0.09	7.064	1.05	4.092
12	0.077	0.002	0.019	0.072	2.193	0.063	-0.20	3.44		0.03	4.067	0.87	3.649

P1: Jan.1st2005-Dec.31th 2012
P2: Jan.,1st2013-Dec, 31th 2015

Period P1: Heavy rainfall (S=1.3 Km)

Er-Rachidia

Month	Ks	Ks.10	Ks*	α	β	<AOD(P1)>	p3	p2	p1	p0	A(%)	wp(cm)	TL
1	0.094	0.003	0.023	0.092	2.041	0.081	0.016	0.41	4.30	0.01	4.846	0.85	3.136
2	0.095	0.003	0.023	0.146	2.133	0.130	0.046	1.00	6.65	0.09	6.956	0.94	3.593
3	0.123	0.003	0.029	0.221	2.071	0.221	0.162	2.21	11.22	0.10	10.980	1.04	4.361
4	0.097	0.003	0.023	0.208	1.666	0.186	0.118	1.76	9.50	0.17	9.455	1.16	4.668
5	0.055	0.001	0.013	0.309	2.378	0.274	0.094	1.51	13.98	0.30	8.662	1.72	4.932
6	0.104	0.003	0.025	0.319	2.402	0.282	0.221	3.11	14.45	0.33	13.371	2.02	5.360
7	0.016	0.001	0.016	0.348	4.125	0.246	0.211	2.99	14.10	0.31	13.032	2.30	5.313
8	0.016	0.001	0.016	0.316	4.339	0.283	0.236	2.89	13.82	0.34	14.260	2.45	5.734
9	0.068	0.002	0.016	0.332	3.142	0.300	0.227	3.10	14.55	0.32	13.144	2.51	5.239
10	0.046	0.002	0.011	0.335	3.532	0.300	0.083	1.35	9.14	0.18	7.242	2.08	4.055
11	0.071	0.002	0.017	0.181	2.440	0.163	0.055	1.08	8.07	0.11	7.238	1.65	3.698
12	0.082	0.002	0.020	0.110	2.053	0.097	0.005	0.61	5.08	0.04	5.551	1.44	3.32

(Remaining P1 city blocks — Oujda, Rabat, S'mara, Ouarzazate — follow the same column structure: Ks, Ks.10, Ks, α, β, <AOD(P1)>, p3, p2, p1, p0, A(%), wp(cm), TL.)*